



Paper

Cite this article: Muto A, Alley RB, Parizek BR, Anandakrishnan S (2019). Bed-type variability and till (dis)continuity beneath Thwaites Glacier, West Antarctica. *Annals of Glaciology* 60(80), 82–90. <https://doi.org/10.1017/aog.2019.32>

Received: 14 June 2019

Revised: 16 September 2019

Accepted: 17 September 2019

First published online: 10 October 2019


Keywords:

Antarctic glaciology; seismic; subglacial exploration geophysics; subglacial processes; subglacial sediments

Author for correspondence:

Atsuhiko Muto, E-mail: amuto@temple.edu

Bed-type variability and till (dis)continuity beneath Thwaites Glacier, West Antarctica

Atsuhiko Muto¹, Richard B. Alley² , Byron R. Parizek^{2,3} and Sridhar Anandakrishnan²

¹Department of Earth and Environmental Science, Temple University, Philadelphia, PA, USA.; ²Department of Geosciences and the Earth and Environmental Systems Institute, The Pennsylvania State University, University Park, PA, USA and ³Geosciences and Mathematics, The Pennsylvania State University DuBois, DuBois, PA, USA

Abstract

Recent seismic measurements from upper Thwaites Glacier indicate that the bed-type variability is closely related to the along-flow basal topography. In high-relief subglacial highlands, stoss sides of topographic highs have a relatively higher acoustic impedance ('hard' bed) with lower acoustic impedance ('soft' till) on lee sides. This pattern is similar to observations of many deglaciated terrains. Subglacial hydraulic-potential gradient and its divergence show a tendency for water to diverge over the stoss sides and converge into the lee sides. Convergence favors a thicker or more widespread water system, which can more efficiently decouple ice from the underlying till. Under such circumstances, till deformation does occur but, fluxes are relatively small. Till carried from the lee sides onto stoss sides of downstream bumps should couple to the ice more efficiently, increasing the ability for transport by till deformation. In turn, this suggests that steady-state till transport can be achieved if the stoss-side till layer is thin or discontinuous. In addition, the large basal shear stress generated in the highlands seems too high for a bed lubricated by a continuous although thin deforming till, suggesting till discontinuity, which would allow debris-laden ice to erode bedrock on stoss sides, supplying additional till for transport.

Introduction

Ice flow is dictated to a large extent by the nature of the bed. Models exist for estimating the basal-slip law from the bed type. When the bed is rigid, made of nondeforming rock ('hard' bed), classical Weertman sliding (Weertman, 1957) is usually applied, in which the basal velocity increases with a low power of the basal shear stress, usually between 1 and 3 (perhaps limited to some maximum stress; Schoof, 2005; Joughin and others, 2019). For a bed made of saturated, deforming till ('soft' bed), observations and experiments show that small strains produce strong nonlinearity (Rathbun and others, 2008), with additional strain leading to extreme nonlinearity approaching perfect plasticity (e.g. Kamb, 1991; Tulaczyk and others, 2001; Rathbun and others, 2008). Experiments have also shown that till deformation is often consistent with the Coulomb-plastic rheology (e.g. Iverson and others, 1998; Tulaczyk and others, 2000), in which the basal shear stress equals the ultimate strength of the till, which is proportional to the effective pressure (ice-overburden pressure minus the subglacial water pressure) (e.g. Cuffey and Paterson, 2010; Tsai and others, 2015).

Despite this accumulated knowledge and the ability to describe the basal-slip law for different bed types, observations of the bed types are scarce, and many glacier and ice-sheet models cannot incorporate variable bed types yet. Models are, therefore, often run with a uniform-bed slip law, most commonly a power-law rule with a low exponent consistent with Weertman sliding (e.g. Pollard and DeConto, 2012; Yu and others, 2018). This leads to significant uncertainties in projections of future sea-level rise because the grounding-line retreat rates of marine ice sheets such as the West Antarctic Ice Sheet can be quite different for nearly plastic versus nearly viscous slip laws (Parizek and others, 2013; Ritz and others, 2015; Brondex and others, 2017).

Active-source seismic surveys can map the bed type (e.g. Smith, 2007; Brisbourne and others, 2017; Kulesa and others, 2017). Recent reflection-seismic investigations in upper Thwaites Glacier showed that along-flow variability in the bed type is closely related to the along-flow basal topography (Muto and others, 2019; M2019 hereafter). The upstream portion of the ~40 km seismic profile revealed a ~10 km-long, relatively flat basin capped by a continuous till layer that is soft (as indicated by its low acoustic impedance Z_b ; $\sim 1.5 \times 10^6 < Z_b < 3.33 \times 10^6 \text{ kg m}^{-2} \text{ s}^{-1}$) and likely deforming, with a few isolated spots of ponded water (Fig. 1). Downstream of the basin, subglacial highlands with rugged topography continue for at least the remaining length of the survey line (~30 km). In these subglacial highlands, stoss sides of topographic highs (bumps) were found to have a relatively higher acoustic impedance ('hard' bed), with lower acoustic impedance ('soft till') on lee sides.

The reflection-seismic method, however, has some limitations; those pertaining to the interpretation of the glacier-bed type were discussed in M2019. A particular limitation of interest here in terms of till continuity is the thin-layer effect, discussed in detail by Booth and others (2012). Briefly, if there is a deforming till layer ('soft' bed) that is $< \sim 2 \text{ m}$ thick ($\sim 1/6$ of a seismic wavelength λ ; in our case $\lambda = 12 \text{ m}$ in till at the P -wave velocity of 1800 m s^{-1}

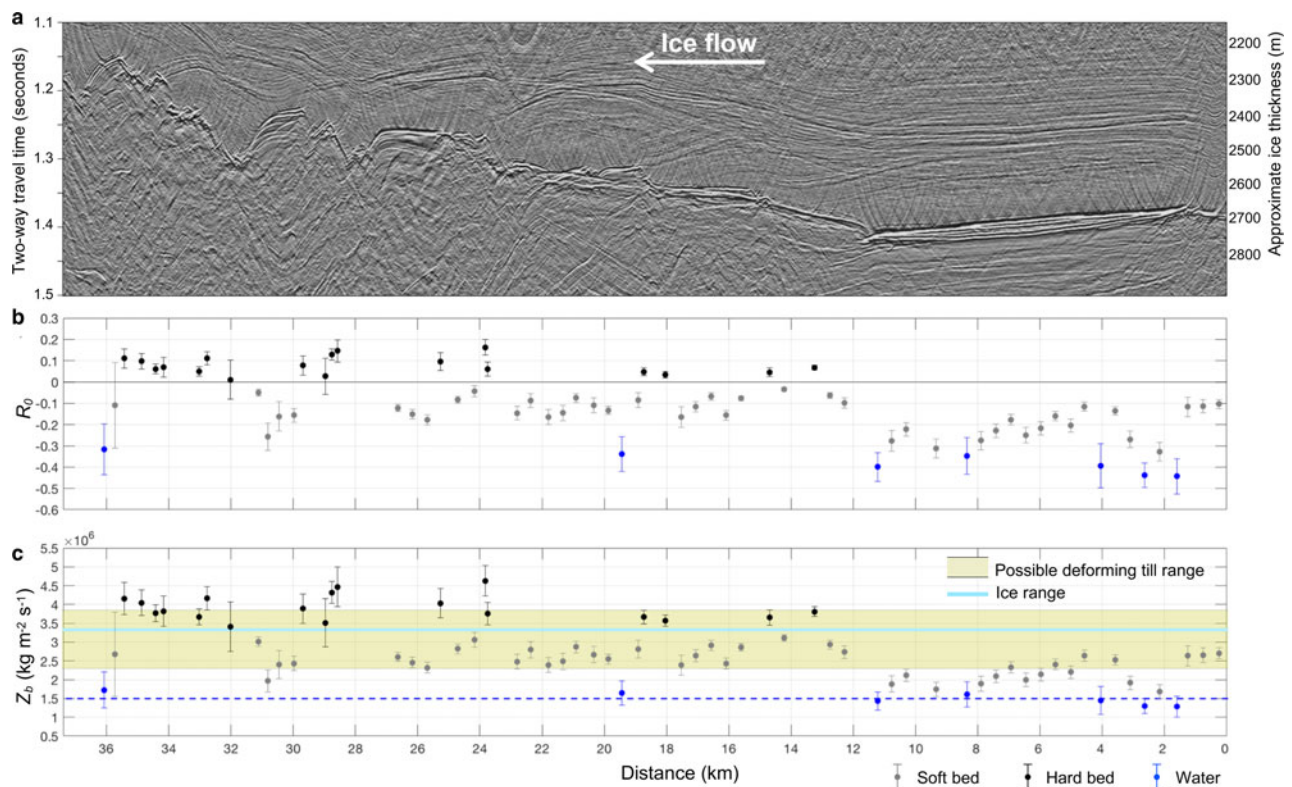


Fig. 1. (a) Stacked, migrated seismic section of the L-line profile along the ice flow. (b) Normal-incidence reflection coefficient (R_0). (c) The bed acoustic impedance (Z_b). Yellow and cyan bands indicate the possible values of deforming till and ice, respectively (Atre and Bentley, 1993). Blue dotted line is the acoustic impedance of water. The interpreted bed type is shown with different colors for each data point. Modified from Muto and others (2019) and used with permission from Elsevier, Earth and Planetary Science Letters.

and the center frequency of 150 Hz) overlying a lodged, low-porosity till layer ('hard' bed), then the apparent reflectivity would be a composite of reflections from the top and the bottom of the deforming till layer and the normal-incidence reflection coefficient would be positive, indicating a hard bed rather than a negative value from a soft till. This leaves the possibility that the hard-bedded stoss sides of topographic highs found by M2019 are in fact covered by seismically thin ($< \sim 2$ m) deforming till. Also, we cannot be certain if the seismic signal for each data point results from a uniform bed or a mix of bed types horizontally over the Fresnel-zone width of the seismic signal (the in-line distance over which the seismic response of the bed is integrated), which in the case of M2019 is ~ 365 m at the average bed depth of ~ 2600 m. The effect of the lateral distribution of bed types is yet to be explored rigorously.

Here, we argue that the regions that appear hard-bedded in the M2019 reflection-seismic data actually include hard-bedded areas, perhaps with patchy thin till, rather than suffering from the thin-layer effect. We rely on three lines of evidence, none of which is unequivocal but which we believe make a strong case together: (i) analogy to deglaciated terrains showing common stoss-side bedrock and lee side till; (ii) physical understanding of continuity of till flux informed by hydrologic calculations based on our data suggesting inadequate till flux from soft-bedded regions to cover roughness on stoss sides of bedrock; and (iii) calculations of basal shear stress supported on different regions of the bed, with large values on stoss sides suggesting interactions with bedrock.

Analogy to deglaciated terrain

Deglaciated terrains can never be perfect analogs for subglacial conditions, both because of differences in conditions during glaciation, and because the imprints of deglaciation and subsequent

changes are lacking beneath active glaciers. Nonetheless, experience shows that knowledge gained from glacial geology informs glaciology (e.g. Boulton, 1976; Stokes and others, 2016).

Deglaciated terrains commonly expose stoss-side rock with lee side till or other sediment, at many scales (e.g. Evans and Hansom, 1996; Ives and Iverson, 2019). Figure 2a shows the stoss side of a bump, ~ 6 to 7 m tall, on Danmark Island, east Greenland. The stoss side of the bump is visible, and ice went up this slope away from the camera, striating and polishing (rock-fall from the face has occurred postglacially). The lee side of this bump is soft sediment, probably till, filled almost to the level of the top of the bump. Figure 2b shows a smaller-scale bedrock bump that was exposed within the last couple of years in front of the rapidly retreating Sólheimajökull in Iceland. Although not shown in the photo, the lee side of this bump has a slope gentler than the stoss side and is made of sediment, indicating sediment accumulation there.

In light of such widespread occurrence of stoss-side bedrock and lee side sediment, it is reasonable to surmise that similar conditions will exist in the subglacial environment.

Till continuity

The data of M2019 show regions of seismically thick till with the acoustic impedance less than that for ice, indicating high porosity and high basal-water pressure (e.g. Peters and others, 2006). Under such conditions, prior work (some of which we summarize below) suggests that the till is deforming, but primarily in a narrow zone close to the base of the ice, and that increasing water supply will decrease till deformation by decoupling the ice from the till.

Thwaites Glacier is within the West Antarctic Rift System and is underlain by thin, stretched crust, likely resulting in elevated



Fig. 2. (a) A stoss-side bedrock exposure in till fields on Danmark Island in east Greenland. Inferred ice flow was into and slightly towards the left of the page. (b) Stoss side of a bedrock bump within a till field in front of Sólheimajökull in Iceland. The ice flow was into the page. Person kneeling down is A. Muto. Both photos were taken by R. Alley.

geothermal flux (Damiani and others, 2014; Schroeder and others, 2014), and there is abundant subglacial water supply (Joughin and others, 2009; Schroeder and others, 2014; Smith and others, 2017). Seismic data of M2019 indicate a thawed bed with abundant water, consistent with these studies.

On Whillans Ice Stream (formerly Ice Stream B), boreholes near where seismic measurements earlier indicated water-saturated deforming till at the bed (Blankenship and others, 1986, 1987) showed water pressures within 2% of flotation, with a few measurements above flotation (Engelhardt and Kamb, 1997; Kamb, 2001). Below one of the boreholes, till deformation was limited to a 3–25 cm layer at the top of the till package, and accounted for only 17% of the total basal motion (Engelhardt and Kamb, 1998; Kamb, 2001). It should be borne in mind, however, that this is a single observation and some large water-pressure fluctuations (up to 1 MPa) were recorded during the observational period (Engelhardt and Kamb, 1998; Alley, 2000), perhaps helping maintain dilatancy to greater depth in the till to produce the seismically thick soft layer (Leeman and others, 2016). Adding water from the boreholes floated the ice off the bed (Kamb, 2001), thus reducing deformation. The weak fabrics within the sediments recovered from beneath Subglacial Lake Whillans, located ~200 km downstream, suggest that the till deformation was within the uppermost 10 cm of the till layer (Hodson and others, 2016), supporting the earlier observations.

Similar relations between the basal-water pressure and ice-till coupling are observed beneath mountain glaciers. Transient observations of water pressure in boreholes and shear strain rate

in till beneath Trapridge Glacier in Canada (Fischer and Clarke, 2001; Kavanaugh and Clarke, 2006) and Storglaciären in Sweden (Iverson and others, 1995) showed reduced shear strain rate when the water pressure rose. Even negative shear strain rates were recorded during some water-pressure peaks (Iverson and others, 1995; Fischer and Clarke, 2001), indicating that the till decoupled from the bed locally and stopped shearing under high water pressure (low effective pressure), responding elastically to reduced shear stress (Iverson and others, 1995, 1999). These changes beneath small alpine glaciers mainly result from water input from the glacier surface, which does not occur on Whillans Ice Stream nor Thwaites Glacier. Nevertheless, reduced ice-till coupling under higher basal-water pressure was consistently recorded and is physically almost inevitable.

We hypothesize that this time-varying behavior also applies to spatial variations along flow in our survey region. As discussed above, increase in water flux is observed to cause a rise in the basal-water pressure, increasing the thickness or area of linked cavities or other features that store and transmit water to balance the greater water flux, and in turn leading to a larger mean thickness of water separating ice and till (Iverson, 1999; Iverson and others, 2007; see review by Alley, 1996). In turn, this may focus stress on a few large clasts that plough the upper part of the till, rather than the ice coupling more widely and driving deeper deformation (Iverson, 1999; Iverson and others, 2007). Therefore, areas of greater water convergence should exhibit greater decoupling between ice and till, and thus less till flux from deformation. This implies that regions of along-ice flow convergence of water have small till flux, whereas along-ice flow divergence of water favors greater till flux. Transitions from water convergence to divergence along ice flow then should increase potential sediment flux, leading to till evacuation, exposing bedrock. A thin deforming layer from soft-bed regions, with deformation, largely occurring over a thickness of order 0.1 m and only where ice and till are not separated by water, would then thin as it was carried into the hard-bed regions, where it would deform more rapidly. Such a layer would be unlikely to bury bedrock topography, and thus likely would be discontinuous in space and perhaps also in time.

We calculated the glaciological hydraulic potential (ϕ) along the main M2019 L-line (Fig. 1), assuming ϕ depends on surface and bed elevations, and that the basal-water pressure is equal to the ice overburden pressure (Shreve, 1972),

$$\phi = \rho_w g z_b + \rho_i g (z_s - z_b) \quad (1)$$

where ρ_w and ρ_i are the densities of water and ice, respectively, g is the gravitational acceleration, and z_s and z_b are the surface and bed elevations, respectively. Surface elevation (z_s) is from the differential GPS data collected concurrently with the seismic data, and bed elevation (z_b) is from the M2019 seismic data. We then calculated the gradient of the hydraulic potential ($d\phi/dx$, the first derivative of the hydraulic potential) and its divergence ($d^2\phi/dx^2$, the second derivative of the hydraulic potential) along the line to find locations where the subglacial water is likely to converge (positive $d^2\phi/dx^2$) or diverge (negative $d^2\phi/dx^2$). The result is shown in Figure 3, with the cross plot of the acoustic impedance (Z_b) and $d^2\phi/dx^2$ in Figure 4.

The pattern of water convergence/divergence and the bed types show a reasonable match with our expectations based on the surface and bed elevations and our current knowledge of the basal slip (e.g. Cuffey and Paterson, 2010; Iverson, 2010), supporting our hypothesis above. In the subglacial highlands (Figs 1a and 3a), $d^2\phi/dx^2$ fluctuates rapidly over several hundred meters to a kilometer along flow, as expected from the more variable surface and bed topographies (Fig. 3d). Negative $d^2\phi/dx^2$ are found over

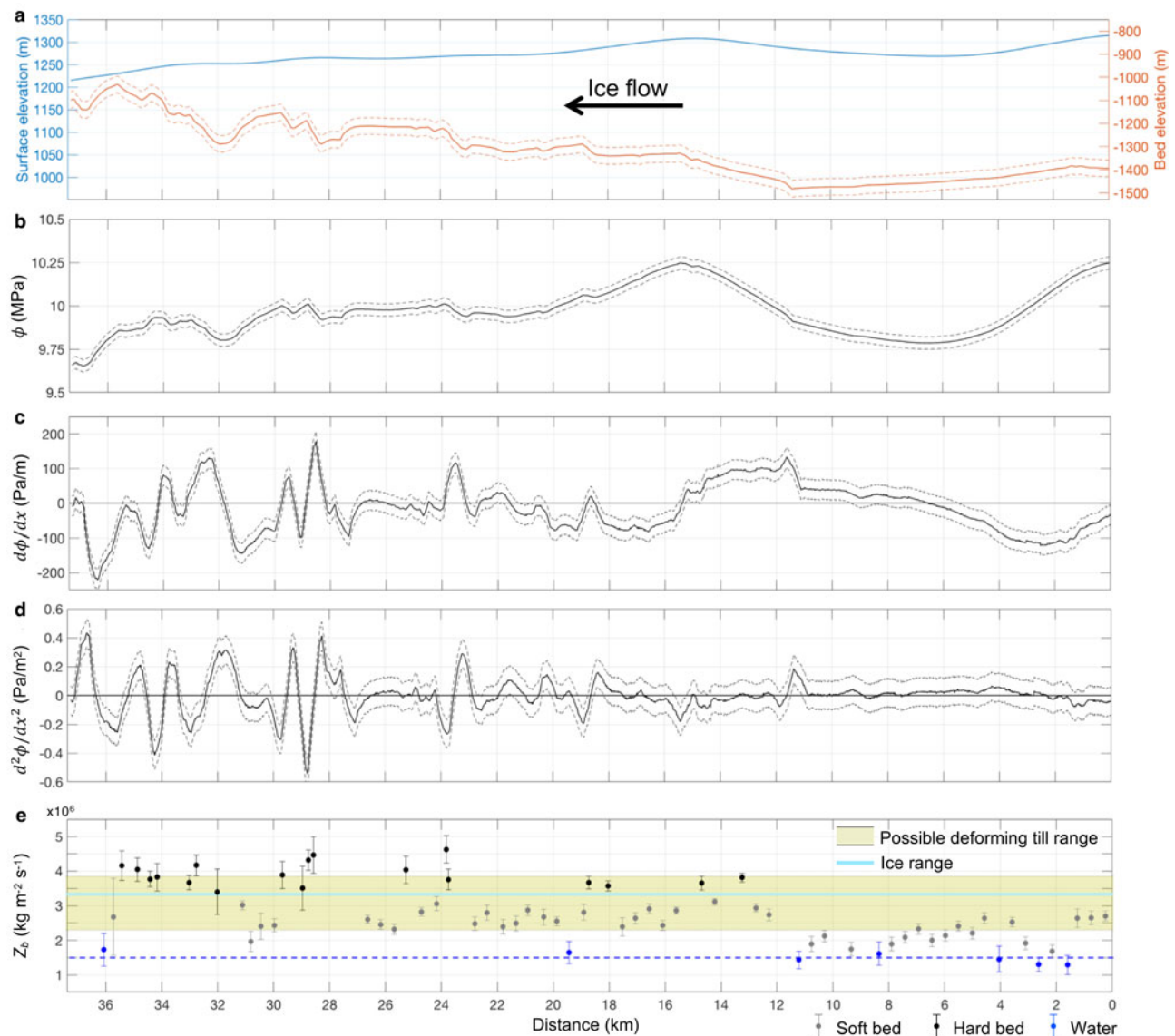


Fig. 3. (a) Surface (blue solid line, left vertical axis) and bed (red solid line, right vertical axis) elevation profiles with the bed-elevation uncertainty (36 m) in red dotted lines. Note that the scale is different for the two profiles and the uncertainty of the surface elevation (10 cm) is negligible. (b) Glaciological hydraulic potential (ϕ). (c) Hydraulic-potential gradient ($d\phi/dx$). (d) Divergence of the hydraulic-potential gradient ($d^2\phi/dx^2$). (e) The bed acoustic impedance (Z_b) and interpreted bed type (same as Fig. 1c).

hard-bedded stoss sides (e.g. 23.5–24.2 km, 28.5–29.1 km and 33.9–34.5 km), seen as a cluster of points with higher Z_b and negative $d^2\phi/dx^2$ in the cross plot (Fig. 4). Positive $d^2\phi/dx^2$ mostly corresponds to soft-bedded lee sides (e.g. 19.5–22 km and 25.5–26.5 km). In the upstream soft-bedded basin, the magnitude of $d^2\phi/dx^2$ is smaller but mostly positive, indicating water convergence, with some of the local maxima corresponding to locations where seismic data indicated water ponding (4 and 11.5 km). The Spearman's rank correlation coefficient (ρ) of the Z_b and $d^2\phi/dx^2$ is -0.48 with the p -value close to 0 (Fig. 4), indicating a weak but significant negative correlation, further supporting our expectation that the hard (soft) bed is associated with water divergence (convergence). We note, however, that the uncertainties of $d^2\phi/dx^2$ include both positive and negative values across this upstream region, suggesting that the correlation of water convergence/divergence with the bed type over the basin may not be as robust as in the downstream highlands.

The acoustic-impedance data were collected at sites spaced mostly ~ 480 m apart and have the Fresnel-zone width of ~ 365 m. However, there are data gaps up to ~ 2 -km long, arising

because of the relatively steep bed slopes where incidence angles of the bed reflections exceeded 10° and the normal-incidence approximation does not hold. This introduces some uncertainty to the interpretation (e.g. 23.2, 28.3 and 33.6 km). We also find regions that are not consistent with our hypothesis (e.g. 13.3–17 km and 29.5–31 km) where $d^2\phi/dx^2$ is negative, indicating water divergence although the seismic data showed soft bed. We cannot tell whether this arises from inadequacies in data, in our assumptions (e.g. out-of-plane water flow), or whether additional processes are active.

Despite these data shortcomings and some mismatches, our results overall suggest that ice will couple more strongly to till on stoss sides than on lee sides, so more till can be carried across stoss sides than is supplied from lee sides. Unless rapid erosion occurs to generate more till (which we discount in part because the stoss sides are still there and have not been worn away), the till then must thin from lee to stoss sides, making it less able to bury small-scale bumps on the stoss sides and favoring a hard-bedded sliding law on the stoss sides alternating with the soft-bedded sliding law on lee sides.

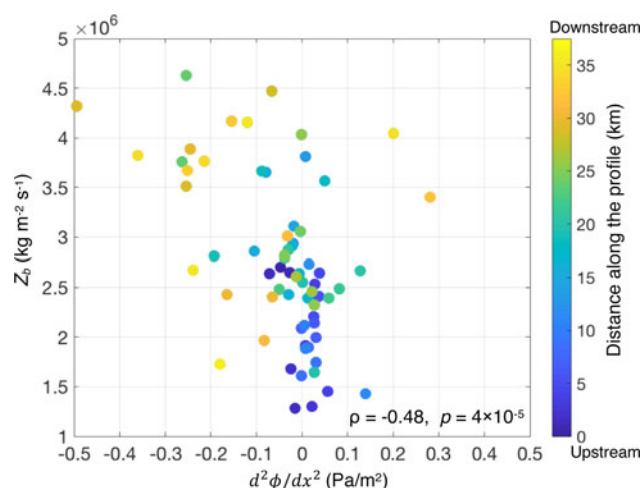


Fig. 4. Cross plot of the acoustic impedance (Z_b) and the divergence of the hydraulic potential gradient ($d^2\phi/dx^2$). The color scale indicates the location of the acoustic-impedance measurements along the seismic survey line. Spearman's rank correlation coefficient (ρ) of Z_b and $d^2\phi/dx^2$ and its p -value are shown.

Basal shear stress

If a thin, deforming till layer was present on stoss sides, it could bury bumps at the sub-meter scale that may be most important in limiting basal sliding (Weertman, 1957) and prevent friction between bedrock and rocks carried in basal ice. In such a case, we would expect relatively low dynamic drag at the bed. In contrast, bedrock not covered by till can support higher dynamic drag.

We performed a simple inversion for the basal shear stress along the M2019 L-line, which is aligned close to the ice flow direction, using observed surface and bed elevations and the surface speed. We used the Pennsylvania State University 2-D higher-order, finite element model (PSU2D, Parizek and others, 2010; Koellner and others, 2019) as the forward model to simulate outlet glacier flow. Within PSU2D, the basal-slip law is represented by a power law:

$$\tau_b = B_b u(b)^{\frac{1}{m}} \quad (2)$$

where τ_b and B_b are the shear stress and drag coefficient, respectively, at the basal interface. The bed exponent m was held constant across the domain with values of either 1 (linear viscous) or 3 (weakly nonlinear) to represent hard bed and 8 (effectively plastic) to represent soft bed. Total basal traction along the ice/bed interface is composed of both form drag arising from variations in bed elevation and dynamic drag associated with the basal shear stress that is supported by the subglacial material.

Surface elevation used here is from the Airborne Topographic Mapper (ATM; Studinger, 2014, updated, 2018) and bed elevation is from the Multi-channel Coherent Radar Depth Sounder (MCoRDS; Paden and others, 2010, updated, 2018) of NASA's Operation IceBridge. A survey line along the ice flow, including over the M2019 L-line, was flown on 11 November 2011. We used these OIB surface and bed elevation data here rather than in situ data from the seismic survey as was done for the hydraulic-potential calculation in order to minimize boundary effects by extending the model domain ~ 85 km upstream and ~ 5 km downstream of the ~ 40 km seismic line. For the surface speed, we used the MEaSUREs InSAR-based velocity (Rignot and others, 2017) interpolated along the OIB data. All of these datasets were interpolated at a 250-m interval along the flowline. This is spatially coarse compared to the individual linked cavities or other

features generally envisioned to transmit basal water (e.g. Iverson, 1999), so the inversion provides a spatial average across such sub-meter to few-meter features.

We inverted for the basal drag by determining the pattern of the basal drag coefficient (B_b) that reduces the misfit between observed and modeled surface speeds. For each rheology tested, we first looked for a uniform B_b value that gives the approximate mean observed surface speed ($\sim 125 \text{ m a}^{-1}$) within the seismic-survey subdomain. We then iteratively adjusted the B_b field along the entire flowline, followed by additional fine-tuning iterations along the subdomain such that the modeled surface speed closely approximated the observed values along the seismic line (within $\sim 7\%$ on average, with misfits as low as $\sim 0.004\%$ and as high as $\sim 24\%$ across the broad region (6–14 km Figs 3a and 5a) of surface-slope reversal). We thereby recover variations of interest in B_b and subsequently τ_b .

The observed and modeled surface speeds, the resulting basal drag coefficient (B_b), and the calculated basal shear stress (τ_b) are displayed for each basal-slip law (m) in Figures 5a–c, respectively. We also plot Z_b and τ_b for each seismic-data location as cross plots for each basal-slip law (Fig. 6). At the broad scale for each m , τ_b shows the expected pattern; basal shear stress is low in the soft-bedded basin, high overall in the highlands with mixed-bed conditions, and increases when bumps are encountered, and Z_b and τ_b have weak, but positive correlation (Fig. 6). Furthermore, τ_b varies more (less) with sharper (gentler) transitions between low and high values for lower (higher) m , reflecting the nature of the nearly viscous (nearly plastic) slip law to concentrate stresses locally (distribute stresses over a larger distance) (Parizek and others, 2013; Koellner and others, 2019).

Within the basin and the initial upslope into the highlands (between 4 and 16.5 km; Fig. 3a), the basal shear stress is essentially zero (Fig. 5c) where the seismic data showed continuous soft bed with a few locations with ponded water (Fig. 5e). Due to positive surface slopes (negative driving stresses; Fig. 5d) across this broad zone, PSU2D underestimates surface speed over this region despite the lack of dynamic drag. This warrants further investigation of transverse flow effects.

Just prior to entering this soft zone, τ_b is elevated within a region where local driving stress reaches $\sim 270 \text{ kPa}$ (Fig. 5d) as ice flows over a ~ 5 -km-long, ~ 45 -m-high bump that begins ~ 2 km upstream of the seismic line. Relatively high basal shear stress here is consistent with the higher acoustic impedance values among the soft-bedded regions, suggestive of deforming but likely lower-porosity soft bed.

In the highlands, sharp increases in τ_b correspond to seismically hard, stoss sides of bumps (e.g. 18.5–19, and 23.5–24 and 28.5–29 km). Also, the longest stretch of high driving stress and τ_b near the downstream end coincides with the longest section of seismically hard bed between 32 and 35.5 km with relatively high acoustic impedance values (except a long data gap at ~ 33 –34 km), supporting our hypothesis. However, there are localized sections such as 19.5–22 km, 25–26.5 km and 30–31 km where τ_b remains high on the lee side of bumps with soft beds. As previously discussed, these may arise from data inadequacies, out-of-plane effects, additional processes or some combination of these; however, we cannot tell at this point which of these possibilities is at play.

Discussion and conclusions

Prior modeling (e.g. Parizek and others, 2013; Koellner and others, 2019) has shown that the stability of the West Antarctic Ice Sheet may depend on the form of the basal-slip law, not just on the magnitude of the basal drag, with nearly linear, nearly plastic and mixed beds giving often significantly different

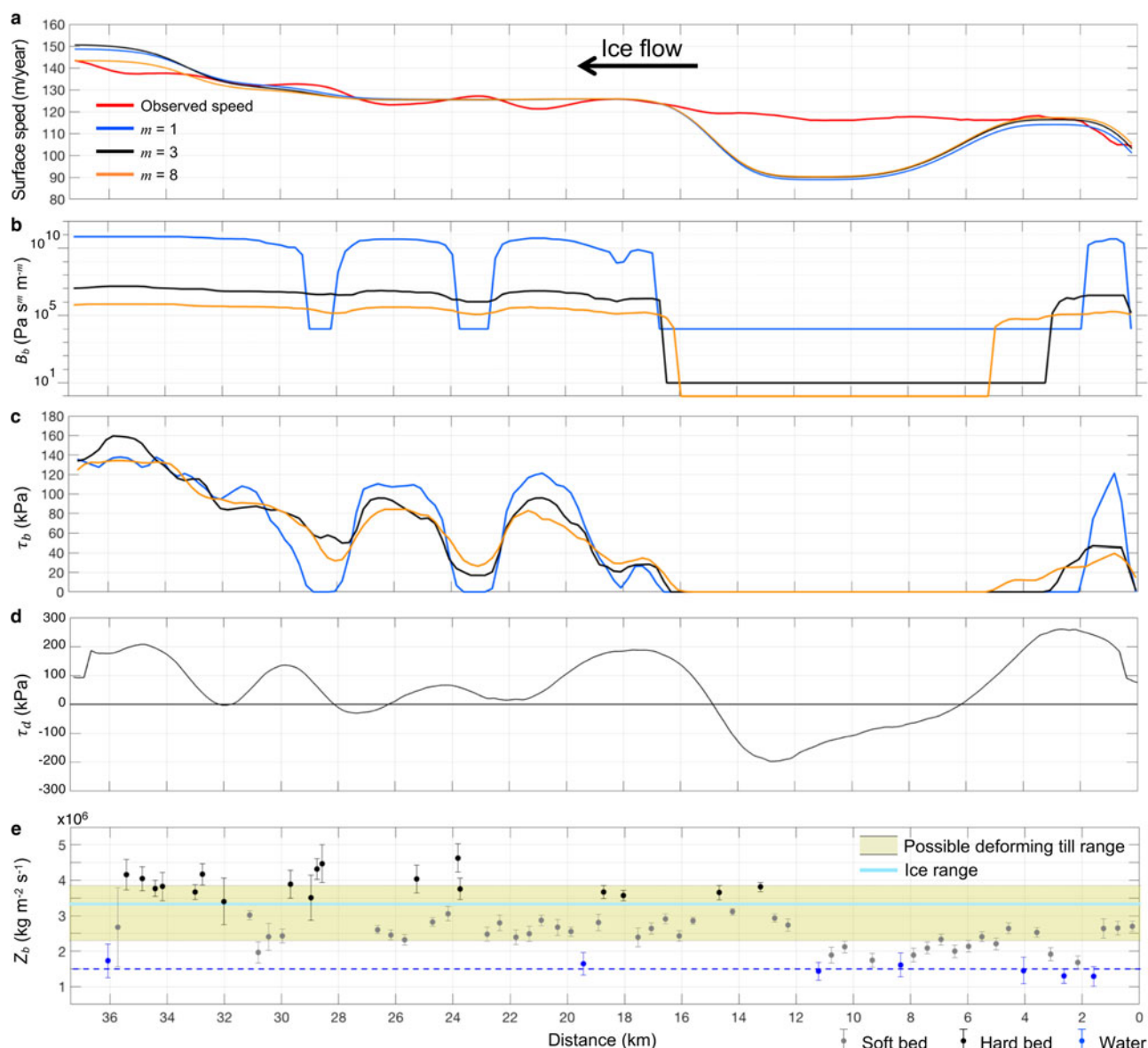


Fig. 5. (a) Observed (red solid line) and modeled (blue, black and orange solid lines) surface speeds. Note that colors for different m values apply to panels b and c. (b) Basal drag coefficient (B_b). (c) Basal shear stress (τ_b). (d) Driving stress (τ_d). (e) The bed acoustic impedance (Z_b) and bed type (same as Fig. 1c).

thresholds for onset of retreat and for subsequent rates of retreat. To a greater extent than most other outlet glaciers such as Siple Coast ice streams (e.g. Anandakrishnan and others, 1998; Peters and others, 2006) and neighboring Pine Island Glacier (Jordan and others, 2010; Smith and others, 2013), Thwaites Glacier flows across the dominant topography rather than along it, giving strongly contrasting basal conditions along flow lines. The simplest interpretation of the seismic data from M2019 indicates that hard and soft beds alternate, with hard stoss sides of elevated bedrock and soft-till lee sides. Prior work, some of which are summarized above, then suggests that basal velocity on stoss and lee sides will obey quite different slip laws that have unique influences on outlet-glacier dynamics in spite of the comparable surface velocities that are observed across these regions (cf. Joughin and others, 2019).

The resolution of seismic data is high but still limited, and it may be physically possible to have a dynamically significant sub-resolution layer of deforming till in regions mapped as hard bed. Whether such a layer can fully bury bedrock roughness has not been studied extensively, but cannot be excluded based on current understanding. Pending such studies, the data indicate that hard

and soft beds alternate along flow, suggesting that the exponent of the basal-slip law alternates along flow, but a continuous soft bed cannot be entirely excluded by the seismic data.

Three lines of evidence presented here suggest that the seismic data accurately capture the basal character. First, the seismic pattern of hard stoss sides and soft lee sides of topography is similar to many deglaciated terrains.

Second, physical understanding and analogy to other subglacial sites indicate that convergence of subglacial water should decouple ice from till, reducing sediment flux by subglacial deformation, whereas divergence of subglacial water should increase ice/bed coupling and till-deformation flux. Our data indicate water convergence over soft-bedded regions and divergence over seismically hard regions. This, in turn, suggests that the sediment flux from soft to hard regions is less than the potential sediment flux across the hard regions. In steady state, a relatively thin (order of 0.1 m) deforming layer from the soft regions overlies a much thicker layer of weakly deforming till. The most-active deforming layer would thin onto the hard regions as coupling to the ice and thus deformation increased, likely becoming discontinuous in space or time, and almost surely

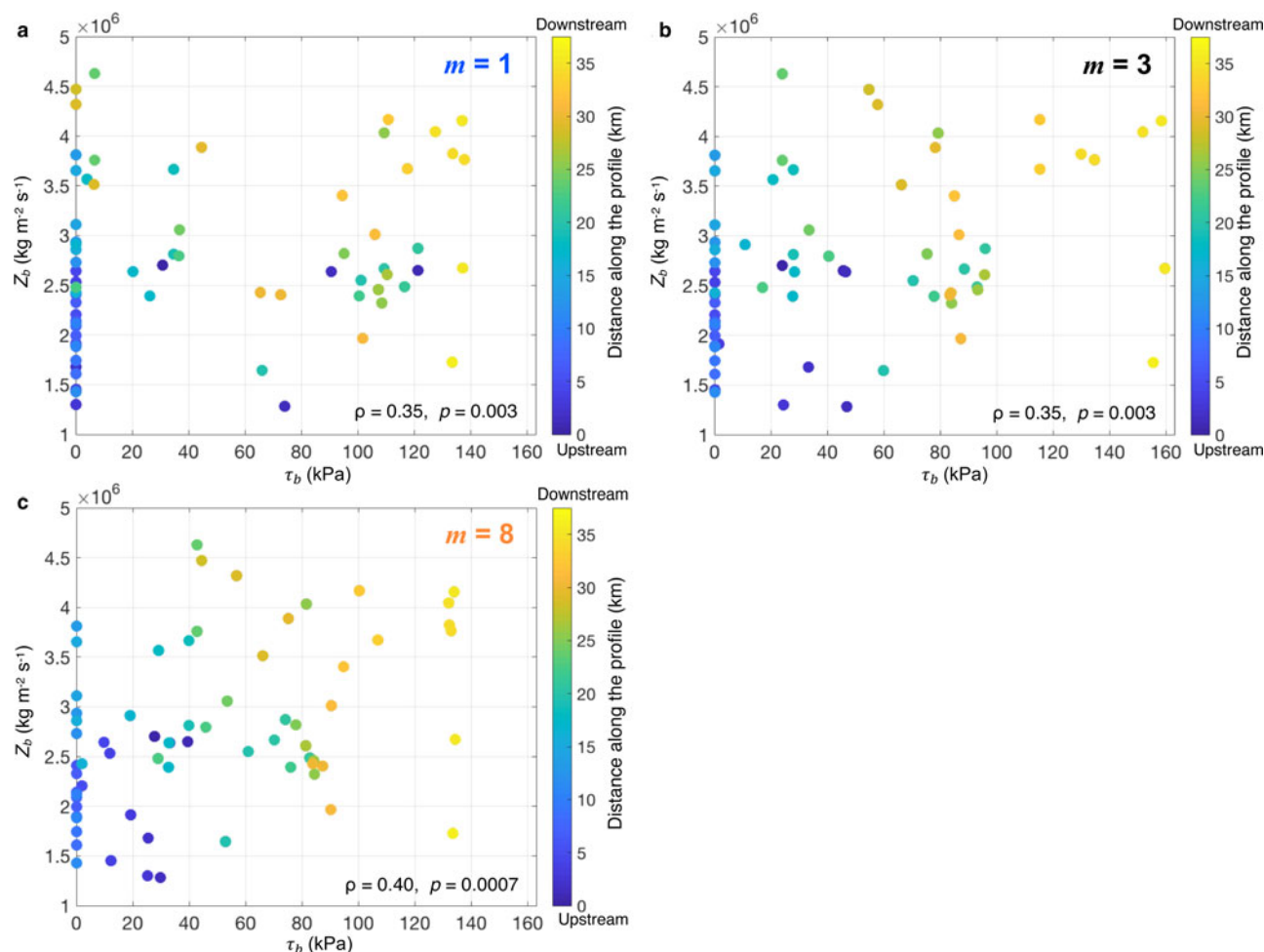


Fig. 6. Cross plots of the acoustic impedance (Z_b) and the basal shear stress (τ_b) for different bed exponent: (a) $m = 1$, (b) $m = 3$ and (c) $m = 8$. The color scale indicates the location of the acoustic-impedance measurements along the seismic survey line. The Spearman's rank correlation coefficient (ρ) of Z_b and τ_b and its p -value for each case of m are shown.

would be insufficient to generate a widespread, continuous soft till layer.

Third, our inversions indicate basal drag in the highlands, especially focused on the stoss sides of the topography that is much higher than can be easily explained by the form drag of the resolved basal topography, indicating large dynamic drag. A soft layer is unlikely to generate such a large, localized drag (note smoothing of the basal shear stress across broader regions for higher bed exponents in Fig. 5c), pointing to interactions between ice or clasts in ice and (rough) bedrock, which requires that soft till be discontinuous or absent on stoss sides.

We note that none of these lines of evidence is unequivocal. Deglaciated bedrock is not a perfect proxy for active subglacial conditions, and there are situations in which stoss-side sediments are observed. We calculated the hydraulic-potential gradient and its divergence only along the ice flow. However, a new high-resolution 3-D basal topographic map created from swath-radar data shows topographic variability across the ice flow; hence the hydraulic-potential gradient may contain a significant across-ice flow component (Holschuh and others, 2019). This may explain mismatches between $d^2\phi/dx^2$ and the expected bed type at some locations. Our datasets were not collected in a perfectly synchronous way (seismic data were collected between December 2008 and January 2009 and IceBridge data were collected in November 2011), and time-evolution may have affected interpretations. More sophisticated inversions for basal drag (e.g. Joughin and others, 2009; Morlighem and others, 2013; Sergienko and

Hindmarsh, 2013) could be conducted. Important along-flow transitions in bed type are observed at a spatial scale that is near the effective resolution of our combined surveys, introducing some uncertainty. Along-flow variations in slope of the ice-air surface likely affect snow accumulation and firn density (e.g. Arcone and others, 2005; Medley and others, 2013), influencing detailed calculations of subglacial hydraulic potential and the local driving stress for viscous ice flow that is ultimately balanced by regional basal drag, lateral drag, and/or ice front conditions.

These and additional considerations are guiding the strategy for planned collection of co-located synchronous reflection-seismic, swath- and snow-radar and surface-velocity data to accurately map 3-D hydraulic potential and its gradient and divergence by the GHOST (Geophysical Habitat of Subglacial Thwaites) project as part of the ongoing ITGC (International Thwaites Glacier Collaboration). The pending success of that effort (currently planned to begin in the 2020–21 Antarctic field season), our results indicate that stoss faces of subglacial topography along Thwaites Glacier are hard-bedded, with soft-bedded lee faces. A full modeling strategy should include a variety of basal-slip laws, but we recommend using the subglacial topography and the results here to specify spatially variable basal-slip laws.

Acknowledgement. This work was supported by the US National Science Foundation under grants NSF-NERC-PLR-1738934 (A.M., R.B.A., B.R.P., S.A.) and PLR-1443190 (B.R.P.), and by the Heising-Simons Foundation

under grant 2018-0769 (R.B.A., B.R.P., S.A.). We thank Alex Brisbourne, an anonymous reviewer and Neal Iverson, the scientific editor, for their constructive reviews that improved the manuscript. This work is from the GHOST project, a component of the International Thwaites Glacier Collaboration (ITGC). Support from National Science Foundation (NSF: Grant NSF-NERC-PLR-1738934) and Natural Environment Research Council (NERC: Grant NE/S006672/1). ITGC Contribution No. ITGC-004.

References

- Alley RB** (1996) Towards a hydrological model for computerized ice-sheet simulations. *Hydrol. Process.*, **10**, 649–660 (doi: 10.1002/(SICI)1099-1085(199604)10:4<649::AID-HYP397>3.0.CO;2-1)
- Alley RB** (2000) Continuity comes first: recent progress in understanding subglacial deformation. *Geol. Soc. London, Special Pub.*, **176**(1), 171–179 (doi: 10.1144/GSL.SP.2000.176.01.13)
- Anandakrishnan S, Blankenship DD, Alley RB and Stoffa PL** (1998) Influence of subglacial geology on the position of a West Antarctic ice stream from seismic observations. *Nature*, **394**, 62–65 (doi: 10.1038/27889)
- Arcone SA, Spikes VB and Hamilton GS** (2005) Stratigraphic variation in polar firn caused by differential accumulation and ice flow: interpretation of a 400-MHz shortpulse radar profile from West Antarctica. *J. Glaciol.*, **51**(7), 407–422 (doi: 10.3189/172756505781829151)
- Atre SR and Bentley CR** (1993) Laterally varying basal conditions beneath Ice Streams B and C, West Antarctica. *J. Glaciol.*, **39**(133), 507–514
- Blankenship DD, Bentley CR, Rooney ST and Alley RB** (1986) Seismic measurements reveal a saturated, porous layer beneath an active Antarctic ice stream. *Nature*, **322**, 54–57 (doi: 10.1038/322054a0)
- Blankenship DD, Bentley CR, Rooney ST and Alley RB** (1987) Till beneath ice stream B: 1. Properties derived from seismic travel times. *J. Geophys. Res.*, **92**(B9), 8903–8911 (doi: 10.1029/JB092iB09p08903)
- Booth AD and 6 others** (2012) Thin-layer effects in glaciological seismic amplitude-versus-angle (AVA) analysis: implications for characterising a subglacial till unit, Russell Glacier, West Greenland. *Cryosphere*, **6**(4), 909–922 (doi: 10.5194/tc-6-909-2012)
- Boulton GS** (1976) The origin of glacially fluted surfaces—observations and theory. *J. Glaciol.*, **17**(76), 287–309 (doi: 10.3189/S0022143000013605)
- Brisbourne AM and 8 others** (2017) Bed conditions of Pine Island Glacier, West Antarctica. *J. Geophys. Res.: Earth Surf.*, **122**, 419–433 (doi: 10.1002/2016JF004033)
- Brondex J, Gagliardini O, Gillet-Chaulet F and Durand G** (2017) Sensitivity of grounding line dynamics to the choice of the friction law. *J. Glaciol.*, **63** (241), 854–866 (doi: 10.1017/jog.2017.51)
- Cuffey KM and Paterson WSB** (2010) *The physics of glaciers*, 4th edn. Butterworth-Heinemann, Oxford.
- Damiani TM, Jordan TA, Ferraccioli F, Young DA and Blankenship DD** (2014) Variable crustal thickness beneath Thwaites Glacier revealed from airborne gravimetry, possible implications for geothermal heat flux in West Antarctica. *Earth Planet. Sci. Lett.*, **407**(C), 109–122 (doi: 10.1016/j.epsl.2014.09.023)
- Engelhardt H and Kamb B** (1997) Basal hydraulic system of a West Antarctic ice stream: constraints from borehole observations. *J. Glaciol.*, **43**(144), 207–230 (doi: 10.3189/S0022143000003166)
- Engelhardt H and Kamb B** (1998) Basal sliding of ice stream B, West Antarctica. *J. Glaciol.*, **44**(147), 223–230 (doi: 10.3189/S0022143000002562)
- Evans DJA and Hansom JD** (1996) The Edinburgh Castle crag-and-tail. *Scott. Geogr. Mag.*, **112**(2), 129–131 (doi: 0.1080/14702549608554461)
- Fischer UH and Clarke GKC** (2001) Review of subglacial hydro-mechanical coupling: Trapridge Glacier, Yukon Territory, Canada. *Quatern. Intern.*, **86**(1), 29–43 (doi: 10.1016/S1040-6182(01)00049-0)
- Hodson TO, Powell RD, Brachfeld SA, Tulaczyk S and Scherer RP and WISSARD Science Team** (2016) Physical processes in Subglacial Lake Whillans, West Antarctica: inferences from sediment cores. *Earth Planet. Sci. Lett.*, **444**(C), 56–63 (doi: 10.1016/j.epsl.2016.03.036)
- Holschuh N, Christianson K, Paden J, Alley R and Anandakrishnan S** (2019) Linking postglacial landscapes and subglacial processes through swath radar imaging at Thwaites Glacier, West Antarctica. in *International Symposium on Glacial Erosion and Sedimentation*, Abstract Number 80A2910, Madison, WI, USA, 12–17 June.
- Iverson NR** (1999) Coupling between a glacier and a soft bed: II Model results. *J. Glaciol.*, **45**(14), 41–53 (doi: 10.3189/S0022143000003026)
- Iverson NR and 7 others** (2007) Soft-bed experiments beneath Engabreen, Norway: regulation infiltration, basal slip and bed deformation. *J. Glaciol.*, **53**(182), 323–340 (doi: 10.3189/002214307783258431)
- Iverson NR** (2010) Shear resistance and continuity of subglacial till: hydrology rules. *J. Glaciol.*, **56**(200), 1104–1114 (doi: 10.3189/002214311796406220)
- Iverson NR, Baker RW, Hooke RL, Hanson B and Jansson P** (1999) Coupling between a glacier and a soft bed: I. A relation between effective pressure and local shear stress determined from till elasticity. *J. Glaciol.*, **45**(149), 31–40 (doi: 10.3189/S0022143000003014)
- Iverson NR, Hanson B, Hooke RL and Jansson P** (1995) Flow mechanism of glaciers on soft beds. *Science*, **267**(5194), 80–81 (doi: 10.1126/science.267.5194.80)
- Iverson NR, Hooyer TS and Baker RW** (1998) Ring-shear studies of till deformation: Coulomb-plastic behavior and distributed strain in glacier beds. *J. Glaciol.*, **44**(148), 634–642
- Ives LRW and Iverson NR** (2019) Genesis of glacial flutes inferred from observations at Múlajökull, Iceland. *Geology*, **47**(5), 387–390 (doi: 10.1130/G45714.1)
- Jordan TA and 6 others** (2010) Aerogravity evidence for major crustal thinning under the Pine Island Glacier region (West Antarctica) *Geol. Soc. Am. Bull.*, **122**(5–6), 714–726 (doi: 10.1130/B26417.1)
- Joughin I and 6 others** (2009) Basal conditions for Pine Island and Thwaites Glaciers, West Antarctica, determined using satellite and airborne data. *J. Glaciol.*, **55**(190), 245–257 (doi: 10.3189/002214309788608705)
- Joughin I, Smith BE and Schoof CG** (2019) Regularized Coulomb friction laws for ice sheet sliding: application to Pine Island Glacier, Antarctica. *Geophys. Res. Lett.*, **46**, 4764–4771 (doi: 10.1029/2019GL082526)
- Kamb B** (1991) Rheological nonlinearity and flow instability in the deforming bed mechanism of ice stream motion. *J. Geophys. Res.*, **96**(1310), 16,585–16,595 (doi: 10.1029/91JB00946)
- Kamb B** (2001) Basal zone of the West Antarctic ice streams and its role in lubrication of their rapid motion. In Alley RB and Bindshadler RA eds. *The West Antarctic ice sheet: behavior and environment*. Antarctic Research Series 77, American Geophysical Union, Washington, DC, 157–199 (doi: 10.1029/AR077p0157)
- Kavanaugh JL and Clarke GKC** (2006) Discrimination of the flow law for subglacial sediment using in situ measurements and an interpretation model. *J. Geophys. Res.*, **111**(F1), F01002 (doi: 10.1029/2005JF000346)
- Koellner S, Parizek BR, Alley RB, Muto A and Holschuh N** (2019) The impact of spatially-variable basal properties on outlet glacier flow. *Earth Planet. Sci. Lett.*, **515**, 200–208 (doi: 10.1016/j.epsl.2019.03.026)
- Kulesa B and 10 others** (2017) Seismic evidence for complex sedimentary control of Greenland Ice Sheet flow. *Sci. Adv.*, **3**, e1603071 (doi: 10.1126/sciadv.1603071)
- Leeman JR, Valdez RD, Alley RB, Anandakrishnan S and Saffer DM** (2016) Mechanical and hydrologic properties of Whillans Ice Stream till: implications for basal strength and stick-slip failure. *J. Geophys. Res.: Earth Surf.*, **121**(7), 1295–1309 (doi: 10.1002/2016JF003863)
- Medley B and 12 others** (2013) Airborne-radar and ice-core observations of annual snow accumulation over Thwaites Glacier, West Antarctica confirm the spatiotemporal variability of global and regional atmospheric. *Geophys. Res. Lett.*, **40**, 3649–3654 (doi: 10.1002/grl.50706)
- Morlighem M, Seroussi H, Larour E and Rignot E** (2013) Inversion of basal friction in Antarctica using exact and incomplete adjoints of a higher-order model. *J. Geophys. Res.: Earth Surf.*, **118**(3), 1746–1753 (doi: 10.1002/jgrf.20125)
- Muto A and 7 others** (2019) Relating bed character and subglacial morphology using seismic data from Thwaites Glacier, West Antarctica. *Earth Planet. Sci. Lett.*, **507**, 199–206 (doi: 10.1016/j.epsl.2018.12.008)
- Paden J, Li J, Leuschen C, Rodriguez-Morales F and Hale R** (2010, updated 2018) IceBridge MCoRDS L2 Ice Thickness, Version 1. Boulder, Colorado, USA, NASA National Snow and Ice Data Center Distributed Active Archive Center (doi: 10.5067/GDQ0CUCVTE2Q) [Accessed on 26 February 2019].
- Parizek BR and 10 others** (2013) Dynamic (in)stability of Thwaites Glacier, West Antarctica. *J. Geophys. Res., Earth Surf.*, **118** (doi: 10.1002/jgrf.20044)
- Parizek BR, Alley RB, Dupont TK, Walker RT and Anandakrishnan S** (2010) Effect of orbital-scale climate cycling and meltwater drainage on ice sheet grounding line migration. *J. Geophys. Res.*, **115**, F01011 (doi: 10.1029/2009JF001325)

- Peters LE and 6 others** (2006) Subglacial sediments as a control on the onset and location of two Siple Coast ice streams, West Antarctica. *J. Geophys. Res.*, **111**(B1), B01302, (doi: 10.1029/2005JB003766)
- Pollard D and DeConto RM** (2012) Description of a hybrid ice sheet-shelf model, and application to Antarctica. *Geosci. Model Dev.*, **5**(5), 1273–1295 (doi: 10.5194/gmd-5-1273-2012)
- Rathbun AP, Marone C, Alley RB and Anandakrishnan A** (2008) Laboratory study of the frictional rheology of sheared till. *J. Geophys. Res.: Earth Surf.*, **113**, F02020 (doi: 10.1029/2007JF000815)
- Rignot E, Mouginot J and Scheuchl B** (2017) MEASUREs InSAR-Based Antarctica Ice Velocity Map, Version 2. Boulder, Colorado, USA, NASA National Snow and Ice Data Center Distributed Active Archive Center (doi: 10.5067/D7GK8F5J8M8R) [Accessed on 26 February 2019]
- Ritz C and 5 others** (2015) Potential sea-level rise from Antarctic ice-sheet instability constrained by observations. *Nature*, **528**, 115–118 (doi: 10.1038/nature16147)
- Schoof C** (2005) The effect of cavitation on glacier sliding. *Proc. Royal Soc. A: Math. Phys. Eng. Sci.*, **461**(2055), 609–627 (doi: 10.1098/rspa.2004.1350)
- Schroeder DM, Blankenship DD, Young DA and Quartini E** (2014) Evidence for elevated and spatially variable geothermal flux beneath the West Antarctic Ice Sheet. *Proc. Nat. Acad. Sci.*, **111**(25), 9070–9072 (doi: 10.1073/pnas.1405184111)
- Sergienko OV and Hindmarsh RCA** (2013) Regular patterns in frictional resistance of ice-stream beds seen by surface data inversion, *Science*, **342**(6162), 1086–1089 (doi: 10.1126/science.1243903)
- Shreve RL** (1972) Movement of water in glaciers. *J. Glaciol.*, **11**(62), 205–214 (doi: 10.3189/S002214300002219X)
- Smith AM** (2007) Subglacial bed properties from normal-incidence seismic reflection data. *J. Environ. Engin. Geophys.*, **12**(1), 3–13 (doi: 10.2113/JEEG12.1.3)
- Smith BE, Gourmelen N, Huth A and Joughin I** (2017) Connected subglacial lake drainage beneath Thwaites Glacier, West Antarctica. *Cryosphere*, **11**, 451–467 (doi: 10.5194/tc-11-451-2017)
- Smith AM, Jordan TA, Ferraccioli F and Bingham RG** (2013) Influence of subglacial conditions on ice stream dynamics: seismic and potential field data from Pine Island Glacier, West Antarctica. *J. Geophys. Res.: Solid Earth*, **118**(4), 1471–1482 (doi: 10.1029/2012JB009582)
- Stokes CR, Margold M and Creyts TT** (2016) Ribbed bedforms on palaeo-ice stream beds resemble regular patterns of basal shear stress (“traction ribs”) inferred from modern ice streams. *J. Glaciol.*, **62**(234), 696–713 (doi: 10.1017/jog.2016.63)
- Studinger M** (2014, updated 2018) IceBridge ATM L2 Icesn Elevation, Slope and Roughness, Version 2. Boulder, Colorado, USA, NASA National Snow and Ice Data Center Distributed Active Archive Center (doi: 10.5067/CPRXXK3F39RV) [Accessed on 26 February 2019].
- Tsai VC, Stewart AL and Thompson AF** (2015) Marine ice-sheet profiles and stability under Coulomb basal conditions. *J. Glaciol.*, **61**(226), 205–215 (doi: 10.3189/2015JoG14J221)
- Tulaczyk S, Kamb B and Engelhardt HF** (2000) Basal mechanics of Ice Stream B, West Antarctica: 1. Till mechanics. *J. Geophys. Res.*, **105**(B1), 463–481 (doi: 10.1029/1999JB900329)
- Tulaczyk S, Kamb B and Engelhardt HF** (2001) Estimates of effective stress beneath a modern West Antarctic ice stream from till preconsolidation and void ratio. *Boreas*, **30**(2), 101–114 (doi: 10.1080/030094801750203134)
- Weertman J** (1957) On the sliding of glaciers. *J. Glaciol.*, **3**(21), 33–38
- Yu H, Rignot E, Seroussi H and Morlighem M** (2018) Retreat of Thwaites Glacier, West Antarctica, over the next 100 years using various ice flow models, ice shelf melt scenarios and basal friction laws. *Cryosphere*, **12**(12), 3861–3876 (doi: 10.5194/tc-12-3861-2018)